THE JOURNAL OF BIOLOGICAL CHEMISTRY VOL. 289, NO. 16, pp. 11293–11303, April 18, 2014


# Function and Regulation of the $Na^+$-$Ca^{2+}$ Exchanger NCX3 Splice Variants in Brain and Skeletal Muscle*

Received for publication, October 23, 2013, and in revised form, February 19, 2014 Published, JBC Papers in Press, March 10, 2014, DOI 10.1074/jbc.M113.529388

**Lauriane Y. M. Michel[‡§], Sjoerd Verkaart[‡], Werner J. H. Koopman[§¶], Peter H. G. M. Willems[§¶], Joost G. J. Hoenderop[‡], and René J. M. Bindels[‡§1]**

*From the Departments of [‡]Physiology and [¶]Biochemistry, [§]Centre for System Biology and Bioenergetics, Radboud University Medical Centre, 6500HB Nijmegen, The Netherlands*

**Background:** The $Na^+$-$Ca^{2+}$ exchanger isoform 3 (NCX3) participates in maintaining calcium homeostasis in brain and skeletal muscle.
**Results:** The two splice variants of NCX3 have distinct regulation and capacity of exchange.
**Conclusion:** Distinct calcium uptake capacity of muscle NCX3 suggests a novel function in muscle exercise physiology.
**Significance:** This study brings a new understanding of the role of NCX3 variants in excitable tissues.

**Isoform 3 of the $Na^+$-$Ca^{2+}$ exchanger (NCX3) is crucial for maintaining intracellular calcium ($[Ca^{2+}]_i$) homeostasis in excitable tissues. In this sense NCX3 plays a key role in neuronal excitotoxicity and $Ca^{2+}$ extrusion during skeletal muscle relaxation. Alternative splicing generates two variants (NCX3-AC and NCX3-B). Here, we demonstrated that NCX3 variants display a tissue-specific distribution in mice, with NCX3-B as mostly expressed in brain and NCX-AC as predominant in skeletal muscle. Using Fura-2-based $Ca^{2+}$ imaging, we measured the capacity and regulation of the two variants during $Ca^{2+}$ extrusion and uptake in different conditions. Functional studies revealed that, although both variants are activated by intracellular sodium ($[Na^+]_i$), NCX3-AC has a higher $[Na^+]_i$ sensitivity, as $Ca^{2+}$ influx is observed in the presence of extracellular $Na^+$. This effect could be partially mimicked for NCX3-B by mutating several glutamate residues in its cytoplasmic loop. In addition, NCX3-AC displayed a higher capacity of both $Ca^{2+}$ extrusion and uptake compared with NCX3-B, together with an increased sensitivity to intracellular $Ca^{2+}$. Strikingly, substitution of $Glu^{580}$ in NCX3-B with its NCX3-AC equivalent $Lys^{580}$ recapitulated the functional properties of NCX3-AC regarding $Ca^{2+}$ sensitivity, $Lys^{580}$ presumably acting through a structure stabilization of the $Ca^{2+}$ binding site. The higher $Ca^{2+}$ uptake capacity of NCX3-AC compared with NCX3-B is in line with the necessity to restore $Ca^{2+}$ levels in the sarcoplasmic reticulum during prolonged exercise. The latter result, consistent with the high expression in the slow-twitch muscle, suggests that this variant may contribute to the $Ca^{2+}$ handling beyond that of extruding $Ca^{2+}$.**

The $Na^+$-$Ca^{2+}$ exchanger (NCX)[2] is a plasma membrane transporter that plays a major role in the maintenance of $Ca^{2+}$ homeostasis in various cell types (1, 2). NCX catalyzes the exchange of $Na^+$ and $Ca^{2+}$ with a 3:1 stoichiometry (3). Depending on the electrochemical gradient across the plasma membrane NCX can either extrude intracellular $Ca^{2+}$ in its forward mode or take up extracellular $Ca^{2+}$ in its reverse mode. The NCX protein contains 10 transmembrane segments and a large central intracellular loop (4–6). The latter was shown to be responsible for the allosteric modulation of the exchanger by $Na^+$ and $Ca^{2+}$ (7). A high intracellular $Na^+$ concentration ($[Na^+]_i$) or low intracellular $Ca^{2+}$ concentration ($[Ca^{2+}]_i$) inactivates the reverse mode of the exchanger (7–9).

In mammals, the NCX family consists of three separate genes: *NCX1*, *NCX2*, and *NCX3* (10). NCX1 is predominantly expressed in heart, kidney, and brain (11), NCX2 is most abundantly expressed in brain (12), and NCX3 is expressed in excitable tissues such as brain and skeletal muscle (13). Numerous splice variants of NCX1 exist in various species, whereas there is only a single variant described for NCX2 (12). Finally, for NCX3, six variants have been described in human (12, 14). In mice, two variants of NCX3 have been identified, but data regarding their expression pattern are lacking. It has, therefore, been hypothesized that expression of mouse NCX3 variants follows the same tissue distribution as that observed in rat (12). This would imply that in mice NCX3-B is expressed in brain, and NCX3-AC expression is restricted to the adult skeletal muscle. These two NCX3 variants are derived from an alternative splicing of the exons A, B, and C. Given the fact that exons A and B are mutually exclusive, the alternative splicing introduces a difference of 24 residues between the NCX3-B and NCX3-AC variants. All of these residues are located within the cytoplasmic regulatory loop known to regulate the activity of the exchanger (12).

The role of NCX3 in brain has been extensively studied. In neurons, NCX3 plays an important role in pathological situations such as ischemia and excitotoxicity (15, 16). In skeletal

* This work was supported by Equipment Grant 911-02-008 from Netherlands Organization for Scientific Research and the Centre for Systems Biology Research Initiative Grant CSBR09/013V from the Netherlands Organization for Scientific Research.
[1] To whom correspondence should be addressed: Dept. of Physiology, Radboud University Medical Center, P.O. Box 9101, 6500 HB Nijmegen, The Netherlands. Tel.: 31-24-3614211; Fax: 31-24-3616413; E-mail: Rene.Bindels@radboudumc.nl.

[2] The abbreviations used are: NCX, $Na^+$-$Ca^{2+}$ exchanger; ER, endoplasmic reticulum; CBD2, $Ca^{2+}$-binding domain 2; CFP, cerulean fluorescent protein.

muscle, NCX3 action constitutes the major $Ca^{2+}$ extrusion mechanism during the relaxation process (17). Its absence induces muscle necrosis and aberrant $Ca^{2+}$ homeostasis (18). However, little is known about the regulation and functional properties of NCX3-B and NCX3-AC.

The aim of the present study was to gain insight into the properties and physiological role of NCX3-B and NCX3-AC. To this end, the expression of both variants in various mouse tissues was assessed. Next, we investigated whether the amino acid differences in the regulatory loop of both NCX3 variants have functional consequences. Therefore, NCX3-AC and NCX3-B were expressed at the plasma membrane in human embryonic kidney (HEK293T) cells. Subsequently, the regulation of the NCX3 variants by $[Ca^{2+}]_i$ and $[Na^+]_i$ was studied using Fura-2-based $Ca^{2+}$ imaging. Finally, the same approach was applied to site-directed mutants to investigate the molecular mechanisms that give rise to the differences in exchange activity.

## EXPERIMENTAL PROCEDURES

*cDNA Cloning*—Murine NCX3-B (kindly provided by Prof. Geerten Vuister, Leicester, UK) was subcloned into the XhoI and NheI sites of the bicistronic mammalian vector pCINeo containing an internal ribosome entry site and enhanced green fluorescent protein. An HA tag was added to the N terminus of the NCX protein. Fragments corresponding to exons AC or B were obtained by amplification of cDNA from mice hind limb skeletal muscle using a high fidelity DNA polymerase (Phusion, Thermo Fisher). The uncut fragment, containing only NCX3-AC, after digestion with XmnI was subcloned into the BlpI and XhoI sites of NCX3-B pCINeo vector. The D1ER calcium sensor targeted to the endoplasmic reticulum (ER) was inserted in a pcDNA3. Following transformation, the plasmids were tested by the action of two-cutter restriction enzymes and subsequently checked by sequencing.

*Mutagenesis*—All NCX3-B mutants were generated using a QuikChange site-directed mutagenesis kit (Stratagene, La Jolla, CA) following the manufacturer's instructions. All mutants were subsequently validated by Sanger sequencing.

*Expression Profile and Quantitative Real-time Polymerase Chain Reaction Analysis*—Three C57BL/6 mice were sacrificed. The brain, heart, and four different skeletal muscles from the hind limb were collected: gastrocnemius, soleus, extensor digitorum longus, and tibialis anterior. Tissue RNA was extracted using TRIzol total RNA isolation reagent (Life Technologies BRL, Breda, The Netherlands). After DNase treatment (Promega, Madison, WI), 1 $\mu$g of RNA was reverse-transcribed by Moloney murine leukemia virus reverse transcriptase (Invitrogen) as described previously (19). Using a CFX96 Real time PCR detection system (Bio-Rad), three calibration curves corresponding to NCX3-AC, NCX3-B, and total NCX3 were realized using serial dilutions of pCINeo-NCX3-B and pCINeo-NCX3-AC. The cDNA from tissues were used to measure the absolute copy number per $\mu$g of mRNA. The sequences were amplified using the following primers: total NCX3, 5′-ATATGGGGAGCTGGAGTTCA-3′ (forward) and 5′-CTGGAGATAACAGGAGCGC-3′ (reverse), NCX3-AC, 5′-GGGCCCCCGCATGGTGGATA-3′ (forward) and 5′-CAGCTTCCTGTCTGTCACTTCTGGA-3′ (reverse), and NCX3-B, 5′-GCATATGGGGAGCTGGAGT-3′ (forward) and 5′-GTTCACCAAGGGCAATGAAG-3′ (reverse).

*Expression of $Na^+/Ca^{2+}$ Exchanger in Human Embryonic Kidney Cells*—Human embryonic kidney cells (HEK293T) were grown in Dulbecco's modified Eagle's medium (Bio Whittaker-Europe, Verviers, Belgium) containing 10% (v/v) fetal calf serum and 2 mM L-glutamine at 37 °C with 5% (v/v) $CO_2$. The cells were seeded on a six-well plate and transiently transfected with the respective constructs (2 $\mu$g/well) using polyethylenimine cationic polymer PEI (Polysciences, Inc., Warrington, PA) in accordance with the manufacturer's instructions. The HEK293T cells were used for the experiments 48 h after transfection.

*Cell Surface Biotinylation*—Cell surface labeling with biotin was performed using the sulfo-NHS-LC-LC-biotin (0.5 mg/ml, Thermo Fisher Scientific, Rockford, IL) as described previously (20). Cells from each six-well plate were homogenized on ice in 0.5 ml of lysis buffer (150 mM NaCl, 5 mM EDTA, 0.5% (v/v) Triton X-100 (v/v), protease inhibitors, 50 mM Tris/HCl, pH 7.5) to prevent endo- and exocytosis, as described previously (21). Subsequently 5% (v/v) of the total protein amount was collected as an input sample. Next, biotinylated proteins (plasma membrane fraction) were precipitated using Neutravidin-agarose beads (Thermo Fisher). Biotinylated fractions were eluted in 2× Laemmli buffer containing 100 mM dithiothreitol and proteinase inhibitors (22). Finally, samples were denatured for 30 min at 37 °C. NCX3-B and NCX3-AC expression was analyzed by immunoblot analysis for the input and the plasma membrane fraction (23).

*Immunoblot Analysis*—Lysates were subjected to SDS-PAGE 8% (w/v) and electroblotted onto PVDF membranes. Blots were incubated with 5% (w/v) nonfat dried milk in TBS-T (137 mM NaCl, 0.2% (v/v) Tween 20, and 20 mM Tris/HCl, pH 7.6). Immunoblots were incubated overnight at 4 °C with a rabbit anti-NCX3 antibody (1:3000) (kindly provided by Prof. Kenneth Philipson, UCLA) (24) diluted in 1% (w/v) milk in TBS-T. PVDF membranes were incubated 1 h at room temperature with a sheep horseradish peroxidase-conjugated anti-rabbit (1:10000) (Sigma) in TBS-T. Afterward, blots were visualized using the enhanced chemiluminescence system (ECL, Thermo Fisher).

*$[Ca^{2+}]_i$ and $[Ca^{2+}]_{ER}$ Measurements*—48 h after transfection, cells were loaded with 3 $\mu$M Fura-2 acetoxymethyl ester (Fura-2/AM) and 0.01% (v/v) Pluronic F-127 for 20 min at 37 °C in Krebs solution (5.5 mM KCl, 147 mM NaCl, 1.2 mM $MgCl_2$, 1.5 mM $CaCl_2$, 10 mM glucose, and 10 mM HEPES/NaOH, pH 7.4). Then, the cells were washed with Krebs medium for 10 min. Finally the coverslips were placed into a perfusion chamber mounted onto the stage of an inverted microscope (Zeiss Axiovert 200 M, Carl Zeiss, Jena, Germany). Changes in medium and addition of inhibitors were facilitated using a perfusion system. $[Ca^{2+}]_i$ was monitored by exciting Fura-2 with monochromatic light of wavelength 340 and 380 nm (Polychrome IV, TILL Photonics, Gräfelfing, Germany). Fluorescence emission light was directed by a 415DCLP dichroic mirror (Omega Optical, Inc., Brattleboro, VT) through a 510WB40 emission filter (Omega Optical, Inc.) onto a CoolSNAP HQ monochrome CCD camera

(Roper Scientific, Vianen, The Netherlands). The integration time of the CCD camera was set at 200 ms with a sampling interval of 3 s. $[Ca^{2+}]_{ER}$ was monitored on cells co-expressing D1ER in a pcDNA3 vector and NCX3 variants in a pCINeo vector lacking the internal ribosome entry site enhanced GFP. cerulean fluorescent protein (CFP) was excited with monochromatic light at 450 nm. Fluorescent emission light was directed by a 455DRLP Dichroic mirror (Omega Optical, Inc.) through 480AF30 and 535AF26 emission filters. All hardware was controlled with Metafluor software (version 6.0, Universal Imaging Corp., Downingtown, PA). During Fura-2 measurements, enhanced GFP-positive cells were selected as transfected cells. During D1ER measurements, CFP-positive cells were selected as cotransfected cells (25). For each wavelength, the mean fluorescence intensity was monitored in an intracellular region and, for purpose of background correction, in an extracellular region of identical size. After background correction, the fluorescence emission ratio (340 nm/380 nm) and (530 nm/480 nm) was calculated to determine the Fura-2 and the D1ER ratios, respectively. Eight to 15 individual cells were selected and monitored simultaneously from each coverslip. NCX activity was evaluated as $Ca^{2+}$ uptake through the reverse mode by switching the normal Krebs medium to a $Na^+$-free NMDG medium containing: 5.5 mM KCl, 147 mM *N*-methyl glucamine, 1.2 mM $MgCl_2$, 1.5 mM $CaCl_2$, 10 mM glucose, and 10 mM HEPES/HCl, pH 7.4 (15). The effect of an increase in $[Ca^{2+}]_i$ and $[Na^+]_i$ was investigated by applying an irreversible and selective inhibitor of the sarcoplasmic reticulum $Ca^{2+}$-ATPase (thapsigargin, 1 $\mu$M) or using an inhibitor of the $Na^+$-$K^+$ ATPase (ouabain, 1 $\mu$M) incubated 60 min prior to the experiment and perfused during recordings as described previously (15). Additionally, the forward mode of the exchanger was evaluated by measuring the capacity to perform $Ca^{2+}$ extrusion after an increase induced by acute addition of the $Ca^{2+}$ ionophore (ionomycin, 1 $\mu$M) in $Ca^{2+}$-free conditions. Osmolality of all buffers has been measured to ensure a difference smaller than 5 mosM. All buffers were kept at 37 °C.

*Analysis of the $[Ca^{2+}]_i$ Measurements*—After initiation of the reverse mode, varying $Ca^{2+}$ uptakes were observed in the different conditions. For each condition, the baseline value was calculated as an average of the first 60 s of recording. During investigation of the forward mode, the baseline Fura-2 ratio recorded in mock-expressing cells in $Ca^{2+}$-free medium was subtracted from the maximal Fura-2 ratio in the same cells after ionomycin treatment. This calculation represents the maximum amount of $Ca^{2+}$ that is present in the ER and that could potentially be extruded via NCX3. Next, the experimental extrusion of $Ca^{2+}$ was calculated as follow: the difference between the mock and the given condition (NCX3-AC, NCX3-B, or mock) both after addition of ionomycin. This difference was reported as a percentage of the theoretical maximum extrusion value described above. This difference is subsequently expressed as a percentage of the theoretical maximal value. During the experiments in absence of thapsigargin or ouabain, the cells responding to a removal of extracellular $Na^+$ were quantified, by taking the Fura-2 ratio value of 0.4 as a threshold of responsiveness.

*Drugs and Chemicals*—Ionomycin and thapsigargin were purchased from Sigma; ouabain was from MP Biomedicals; and Fura-2-AM and pluronic acid were from Invitrogen. All were dissolved in dimethyl sulfoxide. The final concentration of dimethyl sulfoxide was 0.1% (v/v) and had no effect on $[Ca^{2+}]_i$.

*Statistical Analysis*—All results are based on at least three different sessions of experiments. The Fura-2 ratio is an average of ≥65 individual cells. Values are expressed as means ± S.E. Statistical significance ($p < 0.05$) was determined using one-way analysis of variance with Bonferroni's procedure.

## RESULTS

*Expression Profile of NCX3-B and NCX3-AC in Excitable Tissues*—To elucidate the expression of NCX3 variants in excitable tissues, the mRNA expression of NCX3-B and NCX3-AC was quantified in brain, heart, and skeletal muscles. Type I and type II skeletal muscle fibers confer slow-twitch and fast-twitch properties to the myofibers, respectively. In this study, four different skeletal muscles were selected: soleus and extensor digitorum longus for their predominantly constitution of type I and type II fibers, respectively, tibialis anterior, and gastrocnemius for their mixed constitution of fibers in mammals (26). Due to high sequence homology between the two variants, primers were designed to anneal specifically to the alternatively spliced regions corresponding to exons B and AC (Fig. 1, *a* and *b*). A third set of primers was designed to measure the expression of both NCX3 variants. Quantification of total NCX3 expression showed low levels in cardiac tissue, whereas a high expression was measured in brain (Fig. 1*c*). Among the different skeletal muscles, NCX3 was more abundantly found in the slow-twitch muscle fibers constitutive of the soleus than in the fast-twitch or mixed fibers with a 6 to 10-fold difference. In the brain, the expression of NCX3-B was 3-fold higher than NCX3-AC (Fig. 1*d*). In soleus, the opposite trend was observed with NCX3-AC being 3-fold higher than NCX3-B. In the fast-twitch skeletal muscles, NCX3-B was poorly expressed, whereas NCX3-AC expression levels appeared to be >6-fold higher.

*Both NCX3 Variants Display Reverse Mode Exchange Activity*—Next, the investigation of NCX3 functional activity was performed using HEK293T cells transfected with NCX3-AC, NCX3-B, or empty vector (mock). The activity of these exchangers was assessed by measuring changes in $[Ca^{2+}]_i$ using the ratiometric probe Fura-2. Under resting conditions, basal $[Ca^{2+}]_i$ was similar in NCX3-AC, NCX3-B, and mock-transfected cells (Fig. 2*a*). Thapsigargin has been shown to induce a rise in $[Ca^{2+}]_i$ and consequently fully activates NCX (27). Addition of thapsigargin (1 $\mu$M) increased $[Ca^{2+}]_i$ in all three conditions (Fig. 2*a*). However, this increase was significantly lower in cells expressing NCX3-AC (Fig. 2*b*) compared with the other conditions. Removal of extracellular $Na^+$ was used to energize $Ca^{2+}$ uptake via the reverse mode of NCX. This protocol yielded an increase in $[Ca^{2+}]_i$ in cells expressing NCX3-AC and NCX3-B (Fig. 2*c*), indicating reverse mode of exchange activity. Strikingly, the increase in $[Ca^{2+}]_i$ was 3-fold higher in cells expressing NCX3-AC than NCX3-B. Mock-transfected cells failed to respond, indicating that the endogenous NCX expressed in HEK293T cells could not be detected with our method. Cell surface quantification of NCX3 confirmed that

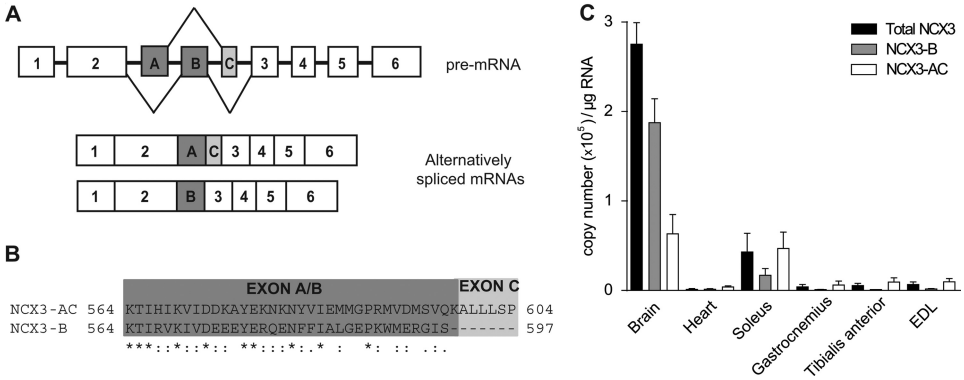


FIGURE 1. **NCX3 splice variants and their tissue expression.** *A*, alternative splicing of the mice $Na^+/Ca^{2+}$ exchanger isoform 3 pre-mRNA and the two variants obtained after alternative splicing of the exons A, B, and C. *B*, alignment of amino acid sequences in alternatively spliced NCX3 exons in the mice NCX3-AC and NCX3-B using ClustalW software. Missing residues are indicated by *dashes*. Symbols *below* the sequence indicate conserved (*period*) highly conserved (*colon*) and identical residues (*asterisk*). *C*, NCX3 mRNA levels in different mice tissues. Total NCX3 (*black*), NCX3-B (*gray*), and NCX3-AC (*white*) transcript expression levels were quantified by real-time PCR. mRNA copy numbers were calculated from the NCX3 standard curves generated by using a diluted pCINeo-IRES-eGFP-mNCX3-AC and pCINeo-IRES-eGFP-mNCX3-B vectors. Heart has been used as a negative control to show the absence of NCX3. *eGFP*, enhanced GFP; *IRES*, internal ribosome entry site. *EDL*, extensor digitorum longus.

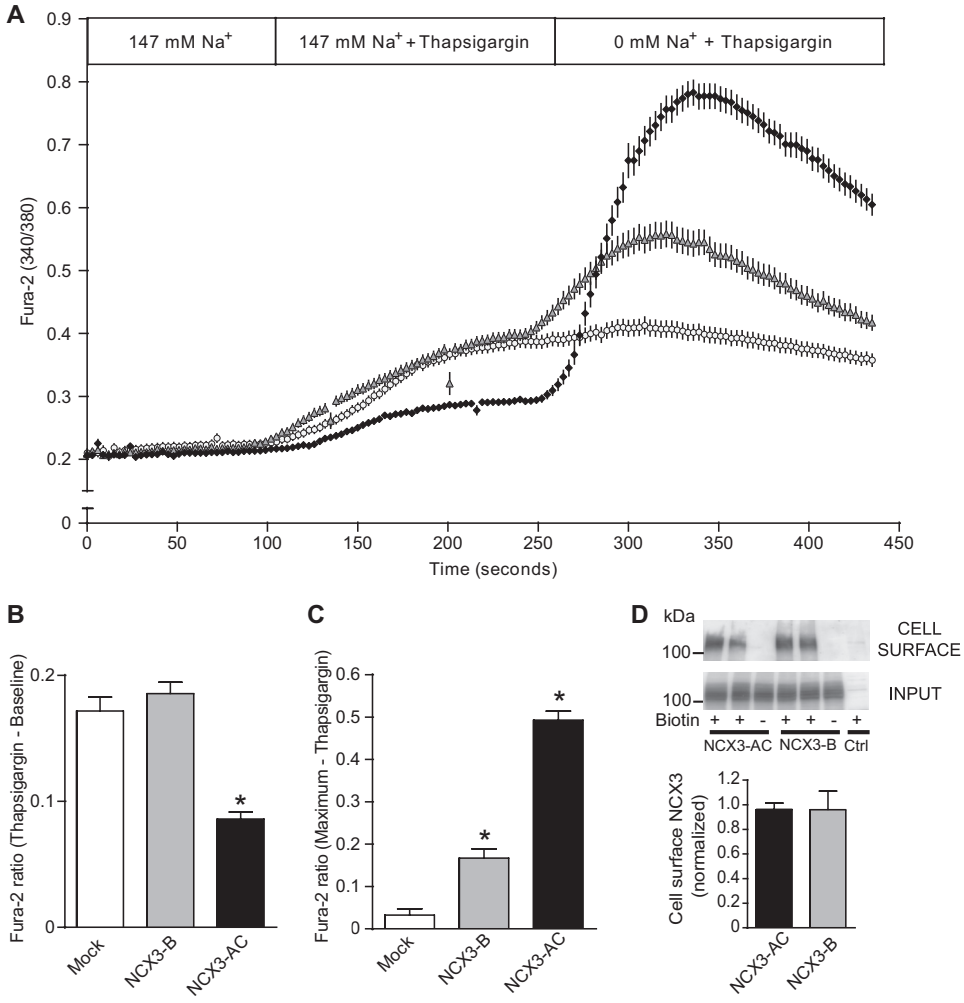


FIGURE 2. **NCX3 variants exhibit functional differences in their reverse mode.** *A*, $Ca^{2+}$ influx in HEK293T cells expressing NCX3-AC (♦), NCX3-B (▲), or an empty vector (○) and loaded with Fura-2-AM. Cells were perfused with Krebs medium (147 mM $Na^+$). At 100 s, internal calcium stores were depleted by applying 1 $\mu$M thapsigargin. At 245 s, reverse NCX mode was initiated by perfusing with a $Na^+$-free medium (NMDG medium). The 340/380 nm emission ratios are shown. Each point represents the mean of the data, studied in three independent experimental sessions for a number (*n*) of cells monitored. Mock, $n = 126$; NCX3-B, $n = 96$; NCX3-AC, $n = 106$. *B*, mean values of the maximum Fura-2 ratio after addition of thapsigargin (1 $\mu$M) shown in *A*. *C*, mean values of the maximum Fura-2 fluorescence shown in *A* after removal of extracellular $Na^+$. *, $p < 0.05$ (*B* and *C*). *D*, quantification and representative immunoblots of total cellular NCX3 at the plasma membrane (cell surface) and in the total cell lysates (*Input*) in cells expressing NCX3-AC, NCX3-B, or an empty vector (*Ctrl*). For each condition, cells that were not treated with biotin are included for comparison ($n = 4$ per condition).

both variants were similarly expressed at the plasma membrane (Fig. 2*d*).

*Forward Exchange Activity of NCX3-AC Is Most Sensitive to Intracellular $Ca^{2+}$*—Furthermore, to explain the reduced increase in $[Ca^{2+}]_i$ upon addition of thapsigargin in NCX3-AC-expressing cells (Fig. 2*b*), we hypothesized that the forward mode of NCX3-AC would be more active, leading to a smaller apparent increase in $[Ca^{2+}]_i$ compared with NCX3-B-expressing cells. In the absence of extracellular $Na^+$ and $Ca^{2+}$, conditions under which the forward mode is abolished, the $Ca^{2+}$ level in the ER and the change in $[Ca^{2+}]_i$ in response to thapsigargin, were similar in all cells (Fig. 3, *a*–*d*).

To strengthen our hypothesis, the forward mode was triggered by perfusing the cells with the $Ca^{2+}$ ionophore ionomycin (1 $\mu$M) in the presence of extracellular $Na^+$. Under these conditions, ionomycin allows for a complete release of $Ca^{2+}$ in a fast manner from the ER to the cytoplasm, thereby inducing an activation of NCX in its forward mode of exchange. Upon addition of ionomycin, an increase in $[Ca^{2+}]_i$ was recorded in the control condition (Fig. 3*e*). This rise in $[Ca^{2+}]_i$ was greatly diminished in both variants of NCX3, confirming the extrusion of $Ca^{2+}$ via the forward mode of the exchanger. The forward mode activity, expressed as the ability to extrude $Ca^{2+}$, was significantly larger for NCX3-AC than for NCX3-B (78 ± 9% and 47 ± 11%, respectively, $p < 0.05$) (Fig. 3*f*).

*The Activity of NCX3-AC in Reverse Exchange Is Higher Than NCX3-B*—Fig. 2, *a* and *c*, show that NCX3-B and NCX3-AC can both operate in the reverse mode and that NCX3-AC induces a larger increase in $[Ca^{2+}]_i$. The capacity of the reverse mode of the NCX3 variants was then investigated by adding thapsigargin in the absence of extracellular $Na^+$, thus preventing a contribution from NCX3 in its forward mode. In these conditions, $[Ca^{2+}]_i$ rose (Fig. 4*a*) in accordance with the pattern seen previously after addition of thapsigargin (Fig. 2*a*). The increase in $[Ca^{2+}]_i$ observed after the switch to the $Na^+$-free condition was significantly higher in NCX3-AC compared with NCX3-B-expressing cells (Fig. 4*b*), pinpointing either a lower sensitivity of NCX3-B to $[Ca^{2+}]_i$ or a poor sensitivity to extracellular $[Na^+]$.

Nevertheless, the $Ca^{2+}$ uptake observed in NCX3-B-expressing cells under removal of extracellular $Na^+$ (Fig. 4*a*) was not detected in the absence of thapsigargin (Fig. 4*c*), demonstrating the importance of intracellular $Ca^{2+}$ in the activation of this variant. In the case of NCX3-AC, a low average was observed (Fig. 4*c*), suggesting a poor activation of the reverse mode. Nevertheless, considering the cells separately, 45% of the NCX3-AC-expressing cells appeared to respond strongly to a change in $Na^+$ gradient (Fig. 4*d*). This effect was less frequent for NCX3-B and mock cells, a response being observed in 7 and 1% of measured cells, respectively (data not shown).

*High Sensitivity of NCX3-AC Reverse Mode to Intracellular $Na^+$*—To investigate the regulation of NCX3 in the reverse mode by intracellular $[Na^+]$, Fura-2 ratios were recorded following incubation of NCX3-AC and NCX3-B-expressing cells with ouabain (1 $\mu$M, 60 min), a $Na^+$,$K^+$-ATPase inhibitor that has been shown to induce a rise in $[Na^+]_i$ (28). An activity in reverse mode was observed for both variants upon removal of extracellular $Na^+$. In both cases, this activity was higher than the one recorded during activation by the increased $[Ca^{2+}]_i$ (Figs. 4*a* and 5*a*). Additionally, the maximum Fura-2 ratio of NCX3-AC in these conditions was found to be significantly higher than recorded in the variant B (Fig. 5*c*).

Surprisingly, after incubation with ouabain, the basal $[Ca^{2+}]_i$ measured in NCX3-AC-expressing cells was found to be very close to the maximum value recorded in the absence of extracellular $Na^+$ (Fig. 5*a*), as demonstrated by the low increase in $[Ca^{2+}]_i$ provoked by the removal of extracellular $Na^+$. The Fura-2 ratio in the presence of extracellular $Na^+$ was observed to be already four times greater than NCX3-B (Fig. 5*b*). This effect was not observed upon activation by intracellular $Ca^{2+}$ (Fig. 4*a*) or in the NCX3-B-expressing cells for which removal of extracellular $Na^+$ seems to be required for the activation of the exchanger. The activation of NCX3-AC by intracellular $[Na^+]$, in high extracellular $Na^+$ condition, demonstrates a much greater sensitivity than NCX3-B to intracellular $Na^+$.

*Molecular Determinants of the $Na^+$ and $Ca^{2+}$ Sensitivity of NCX3 Variants*—The data recorded in Fig. 4 and 5 demonstrated that the NCX3-AC variant is more sensitive to intracellular $Ca^{2+}$ and $Na^+$. To get a better understanding of the molecular mechanisms responsible for this increased sensitivity, the role of several residues of the alternatively spliced region of NCX3 variants was investigated. This region, located in the intracellular loop, within the $Ca^{2+}$-binding domain 2 (CBD2) of the protein, differs significantly from one variant to the other. For instance, negatively charged residues such as glutamate and aspartate found in NCX3-B sequence are absent in NCX3-AC (Fig. 6*a*). These residues have been shown to participate in the formation of the $Ca^{2+}$-binding site of NCX1 (29). Furthermore, at these positions, several positively charged residues are present in the variant AC, residues that are described in the case of NCX1 as critical for stabilization of the tertiary structure of the CBD2 (30, 31).

To study the possible role of these residues in the regulation of the exchanger, site-directed NCX3-B mutants were generated targeting different glutamate residues (Fig. 6*a*) E573D, E574K, E575A, E580K, and E588G. The different mutants were subjected to recording of the forward and the reverse mode by applying the similar protocols as described in the aforementioned paragraphs. Interestingly, E580K NCX3-B displayed similar properties compared with NCX3-AC in both forward and reverse mode (Fig. 6, *b* and *c*) triggered by an elevation in $[Ca^{2+}]_i$. With respect to the activation of the reverse mode through a rise in $[Na^+]_i$, the measurements of the Fura-2 ratio at basal and maximum level revealed a significant increase in the sensitivity to $[Na^+]_i$ in $Na^+$ conditions for four of the five mutants tested (Fig. 6*d*). In the absence of extracellular $Na^+$, only the mutation E573D showed a significant increase in the maximum $[Ca^{2+}]_i$ recorded (Fig. 6*e*). However, the four mutations accounting for the increase seen in Fig. 6*d* displayed, in $Na^+$-free conditions, a trend toward a $Ca^{2+}$ influx similar to NCX3-AC. Furthermore, the comparison between NCX3-AC and the three mutations E573D, E574K, and E580K did not reveal any significant difference. Note that in all four conditions, E588G NCX3-B showed no difference in its capacities compared with NCX3-B.

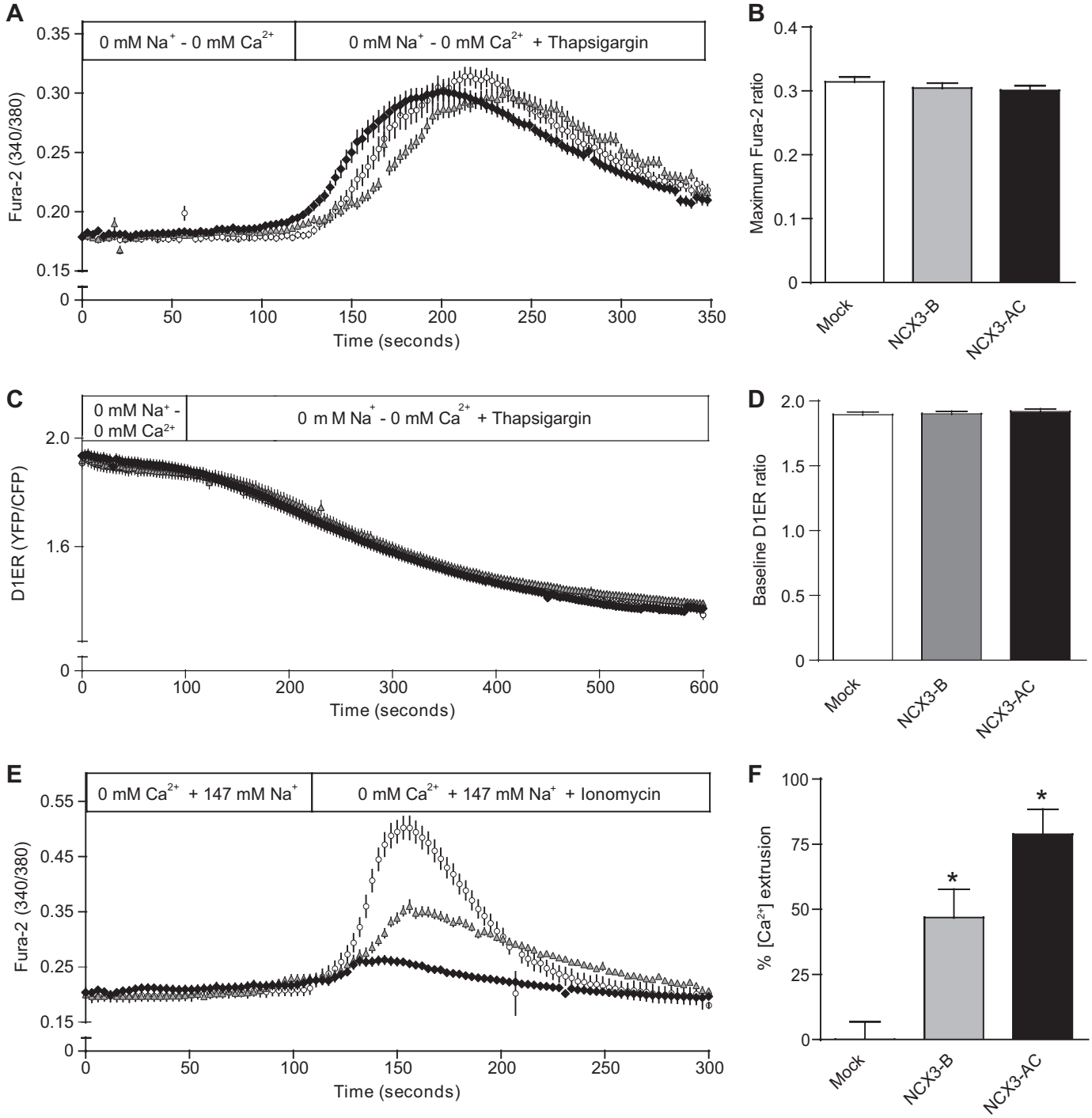


FIGURE 3. **Differences in threshold of activation of the NCX3 variants in the forward mode.** *A–D*, release of $Ca^{2+}$ from the ER in HEK293T cells expressing NCX3-AC (◆), NCX3-B (▲), or an empty vector (○) during perfusion of thapsigargin (1 $\mu$M) in $Na^+$ and $Ca^{2+}$-free conditions after loading and recording of the Fura-2 ratio (340 nm/380 nm) (*A*) and after recording of the D1ER sensor (*C*). Each point represents the mean (± S.E.) of the data, for a number (*n*) of cells monitored. Mock, $n = 72$; NCX3-B, $n = 85$; NCX3-AC, $n = 114$ (in *A*). Mock, $n = 119$; NCX3-B, $n = 99$; NCX3-AC, $n = 150$ (in *C*). *B*, mean values of the maximum Fura-2 ratio after addition of thapsigargin (1 $\mu$M) shown in *A*. *D*, average value of the baseline YFP/CFP ratio shown in *C*. *E*, Fura-2 ratio (340 nm/380 nm) in HEK293T cells expressing NCX3-AC (◆), NCX3-B (▲), or an empty vector (○) during perfusion of ionomycin (1 $\mu$M) in $Ca^{2+}$-free conditions. Each point represents the mean of the data, for a number (*n*) of cells monitored. Mock, $n = 111$; NCX3-B, $n = 78$; NCX3-AC, $n = 94$. *F*, percentage of $[Ca^{2+}]$ extrusion after addition of ionomycin (1 $\mu$M) shown in *A* and calculated as described under "Experimental Procedures." *, $p < 0.05$.

## DISCUSSION

In the present study, we show, for the first time, functional recordings of the variant NCX3-AC. These recordings indicate a higher capacity of this variant in reverse and forward mode of exchange compared with NCX3-B. A difference that can be fully attributed to the intrinsic properties of both variants considering that the plasma membrane expression in HEK293T cells did not differ between the two variants and that the $Ca^{2+}$ level in the endoplasmic reticulum were similar in these cells as proven by the thapsigargin addition in absence of extracellular

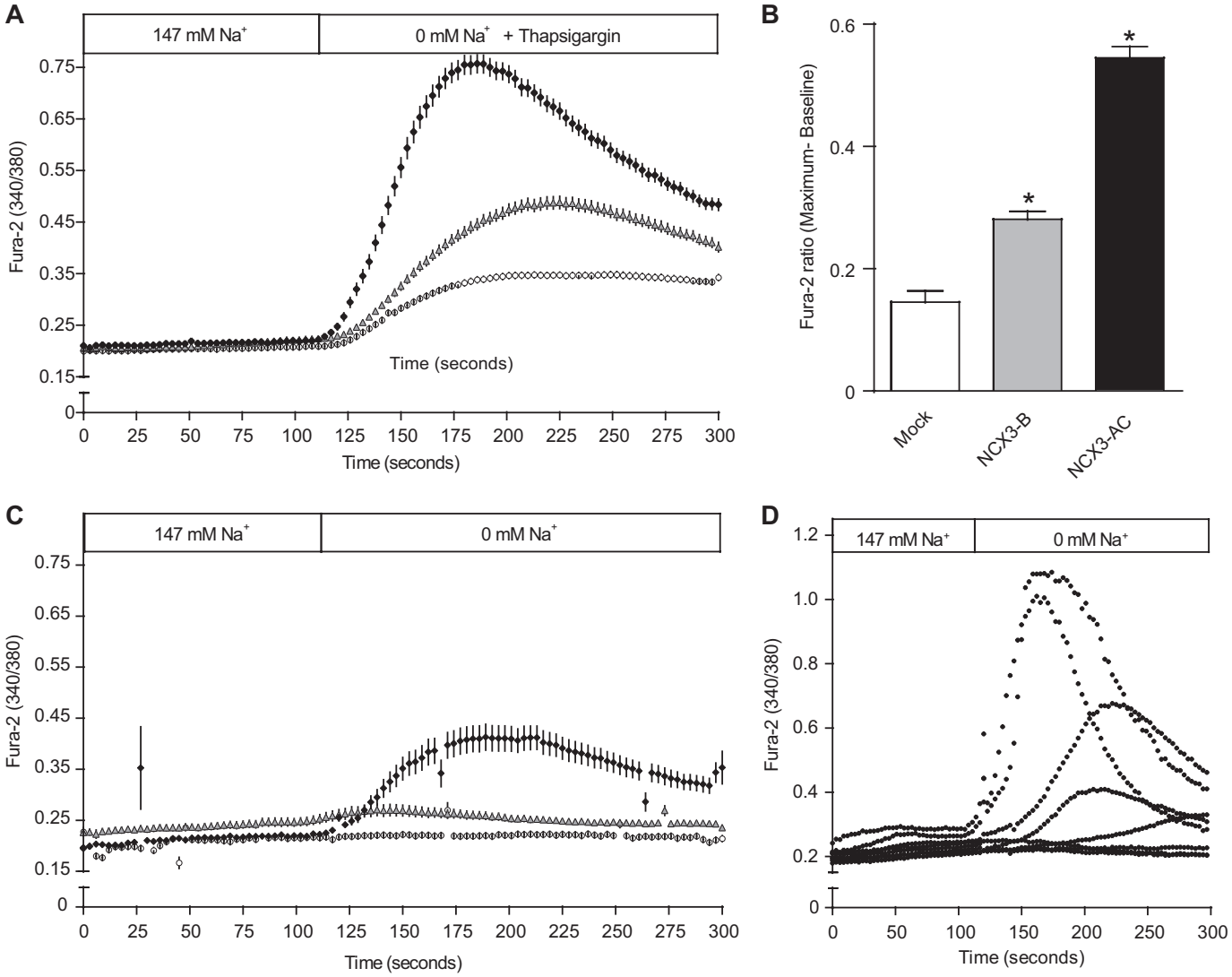


FIGURE 4. **Differences in properties of NCX3-B and NCX3-AC in the reverse mode of exchange.** *A*, $Ca^{2+}$ influx in HEK293T cells expressing NCX3-AC (♦), NCX3-B (▲), or an empty vector (○) in $Na^+$-free conditions simultaneously with applying thapsigargin (1 $\mu$M), conditions for which forward mode exchange is abolished. Mock, $n = 158$; NCX3-B, $n = 153$; NCX3-AC, $n = 139$. *B*, mean values of the maximum Fura-2 ratio after the switch to $Na^+$-free medium containing 1 $\mu$M thapsigargin shown in *A* (*, $p < 0.05$). *C*, Fura-2 ratio in cells expressing NCX3-AC (♦), NCX3-B (▲), or an empty vector (○) in $Na^+$-free conditions in absence of thapsigargin. Each point represents the mean of the data, for a number (*n*) of cells monitored. Mock, $n = 88$; NCX3-B, $n = 66$; NCX3-AC, $n = 104$. *D*, representative recording of eight HEK293T cells expressing NCX3-AC during removal of extracellular $Na^+$ in absence of thapsigargin.

$Na^+$ and $Ca^{2+}$. Furthermore, the reduced $[Ca^{2+}]_i$ measured in NCX3-AC-expressing cells upon thapsigargin addition compared with NCX3-B, together with the activation of NCX3-AC reverse mode in absence of an elevation in $[Ca^{2+}]_i$ suggest a higher sensitivity of NCX3-AC to changes in $[Ca^{2+}]_i$. Thereby, a value slightly above the $[Ca^{2+}]_i$ recorded during the resting state is sufficient to trigger the exchanger.

The lower sensitivity of NCX3-B to $[Ca^{2+}]_i$, in both modes of exchange, could be suppressed by mutating the glutamate residue at position 580. This gain of sensitivity observed in the E580K NCX3-B mutant reveals that the activation by $Ca^{2+}$ of the forward and reverse mode of the exchanger is regulated through the same site for which the residue 580 represents a key residue. In NCX1, the equivalent residue $Lys^{585}$ is involved in the formation of a salt bridge that, in $Ca^{2+}$-free conditions, stabilizes the $Ca^{2+}$-binding site I and II through the preservation of the tertiary structure (29, 32). NCX1 mutation of this lysine into a glutamate causes a drop in the $Ca^{2+}$ affinity (29, 32). In NCX3-AC, $Lys^{580}$ confers to the site I of the CBD2 a high affinity for $Ca^{2+}$ (31–33). In contrast, this variant has two $Ca^{2+}$-binding sites in its $Ca^{2+}$-binding domain 2, whereas isothermal titration calorimetry measurements showed that NCX3-B has three $Ca^{2+}$-binding sites (30, 33). However, none of these $Ca^{2+}$ sites featured a high affinity for $Ca^{2+}$ (33). Our data concur with the literature in suggesting that during a rise in $[Ca^{2+}]_i$, the high-affinity site I of NCX3-AC CBD2 will bind $Ca^{2+}$ at a lower concentration than NCX3-B. This could result in a disruption of the salt bridge at $Lys^{580}$ as hypothesized for NCX1 (29) and, therefore, in an activation of the exchanger at lower $[Ca^{2+}]_i$.

Another important finding from the current study is that NCX3-B displayed a higher $Na^+$-dependent inactivation, given that only the reverse mode of NCX3-AC could be activated, during a rise in $[Na^+]_i$ in presence of extracellular $Na^+$. The partial suppression of this effect by mutating glutamate resi-

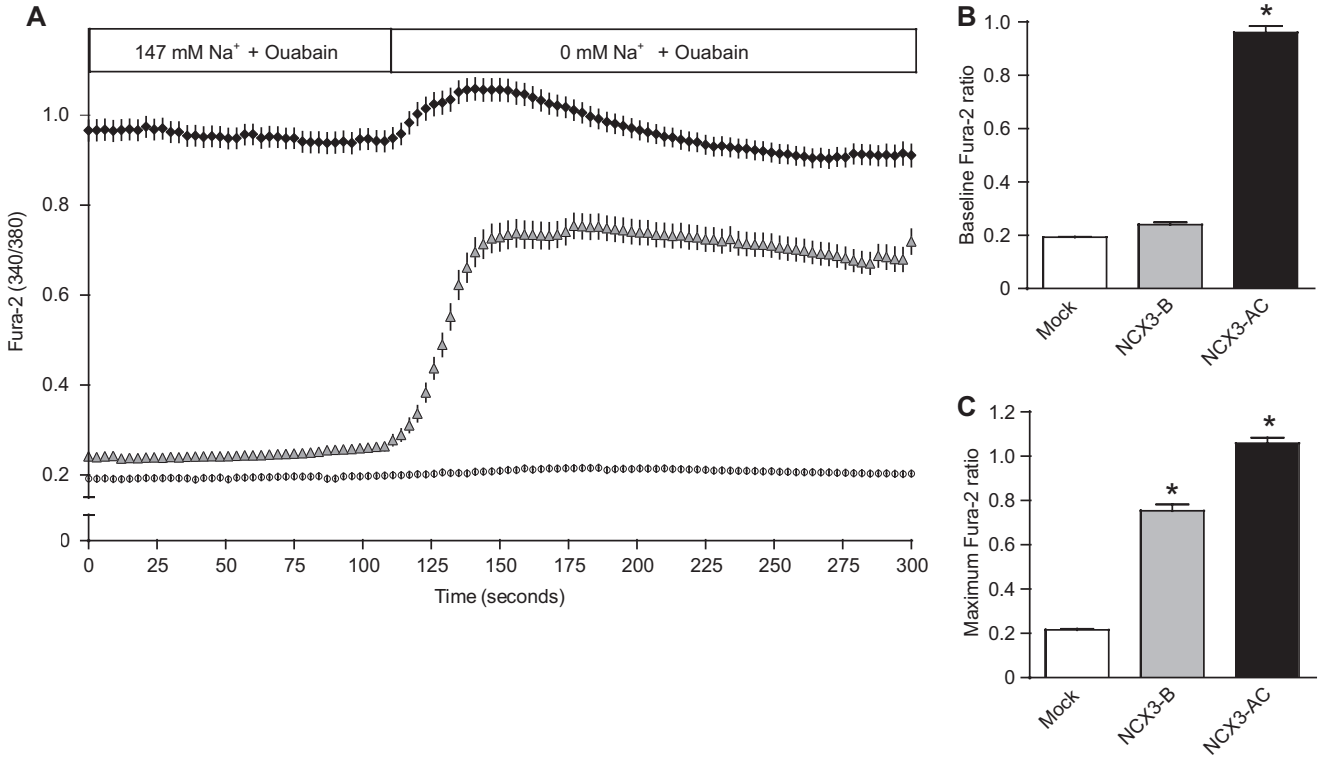


FIGURE 5. **NCX3 variants exhibit distinct sensitivities to $[Na^+]_i$.** *A*, Fura-2 ratio (340 nm/380 nm) in HEK293T cells expressing NCX3-AC (♦), NCX3-B (▲), or an empty vector (○) after 1-h treatment with ouabain (1 $\mu$M). Each point represents the mean of the data, for a number (*n*) of cells monitored. Mock, $n = 124$; NCX3-B, $n = 152$; NCX3-AC, $n = 176$. *B* and *C*, mean values of Fura-2 ratio recorded at the baseline (*B*). Shown is the average of the first 60 s of the experiment shown in *A*, in 147 mM $Na^+$ medium, and maximum Fura-2 ratio recorded after the switch to $Na^+$-free medium shown in *A* (*C*) (*, $p < 0.05$).

dues suggests that the hydrophilic domain found between positions 572 and 580 in the CBD2 domain is involved in this inactivation. For NCX1, it has been demonstrated that the alternative splicing of the same region can alleviate the $Na^+$-dependent inactivation (34, 35). Moreover, D578R and K585C mutations in NCX1, corresponding to positions 573 and 580 in NCX3, reversed the $Na^+$-dependent inactivation in a complete and partial manner, respectively (36). The emerging hypothesis concerning the functioning of this $Na^+$-dependent inactivation is a regulation by the $Ca^{2+}$-binding site of the CBD2 through proximity with the catenin-like domain of the protein (32). This domain, formed by residues of the intracellular loop outside of CBD1 and CBD2, would control the $Na^+$-dependent inactivation. Our results are consistent with the hypothesis predicting that E573D, E574K, E575A, and E580K NCX3-B are responsible for the partial disruption of a $Ca^{2+}$-binding site that will alter the interaction with the catenin-like domain of the protein and, therefore, lower the $Na^+$-dependent inactivation.

The tissue-specific distribution observed for the two variants of NCX3, with NCX3-B as mostly expressed in the brain and with NCX3-AC as the main variant detected in skeletal muscle, is consistent with the functional properties measured for these variants. In neurons, NCX3-B and its low capacity to perform $Ca^{2+}$ uptake would have a protective effect against severe $Ca^{2+}$ overload, a phenomenon that could have dramatic consequences on neurons. With this respect, the low sensitivity to an increase in $[Na^+]_i$ would confer this preservation during the firing of neurons. In the same manner, activation of the forward mode of NCX3-B requires a substantial rise in $[Ca^{2+}]_i$. This feature would have the same protective effect and yet will not interfere with the synaptic activity, highly dependent on $[Ca^{2+}]_i$ (37).

In skeletal muscle, sensitivity to $[Ca^{2+}]_i$ and the high capacity of NCX3-AC in the forward mode corroborates with the necessity in such fibers to activate the $Ca^{2+}$ extrusion as soon as the contraction starts. Moreover, the high sensitivity of NCX3-AC to changes in $[Na^+]_i$ and its high capacity to perform $Ca^{2+}$ uptake in reverse mode suggest that NCX3-AC might have additional implications via its reverse mode. The operation and relevance of the reverse mode has been previously observed for several members of the NCX family in numerous tissues, in both physiological (38–40) and pathological situations (41, 42). From another angle, during prolonged exercise, extracellular $Ca^{2+}$ has been shown to have a beneficial effect on the resistance to muscle fatigue, an effect that could only be observed in slow-twitch muscle, similar to soleus, dedicated to this type of prolonged exercise (43, 44). Together with the high expression of NCX3-AC observed in soleus, these results suggest that NCX3-AC might be implicated in $Ca^{2+}$ influx in slow-twitch muscle, a hypothesis consistent with the findings from Danieli-Betto's group (44). Here, the $Ca^{2+}$-free conditions provoke a dramatic increase of muscle fatigue in soleus, an effect also obtained by inhibition of NCX. This is also in accordance with the increased fatigability observed in $NCX3^{-/-}$ mice (18). The underlying mechanism linking $Ca^{2+}$ uptake and muscle fatigue is still poorly understood but presumably involves a refilling of the SR $Ca^{2+}$. Many variants of the NCX family are already known to contribute to this latter process (45, 46), particularly

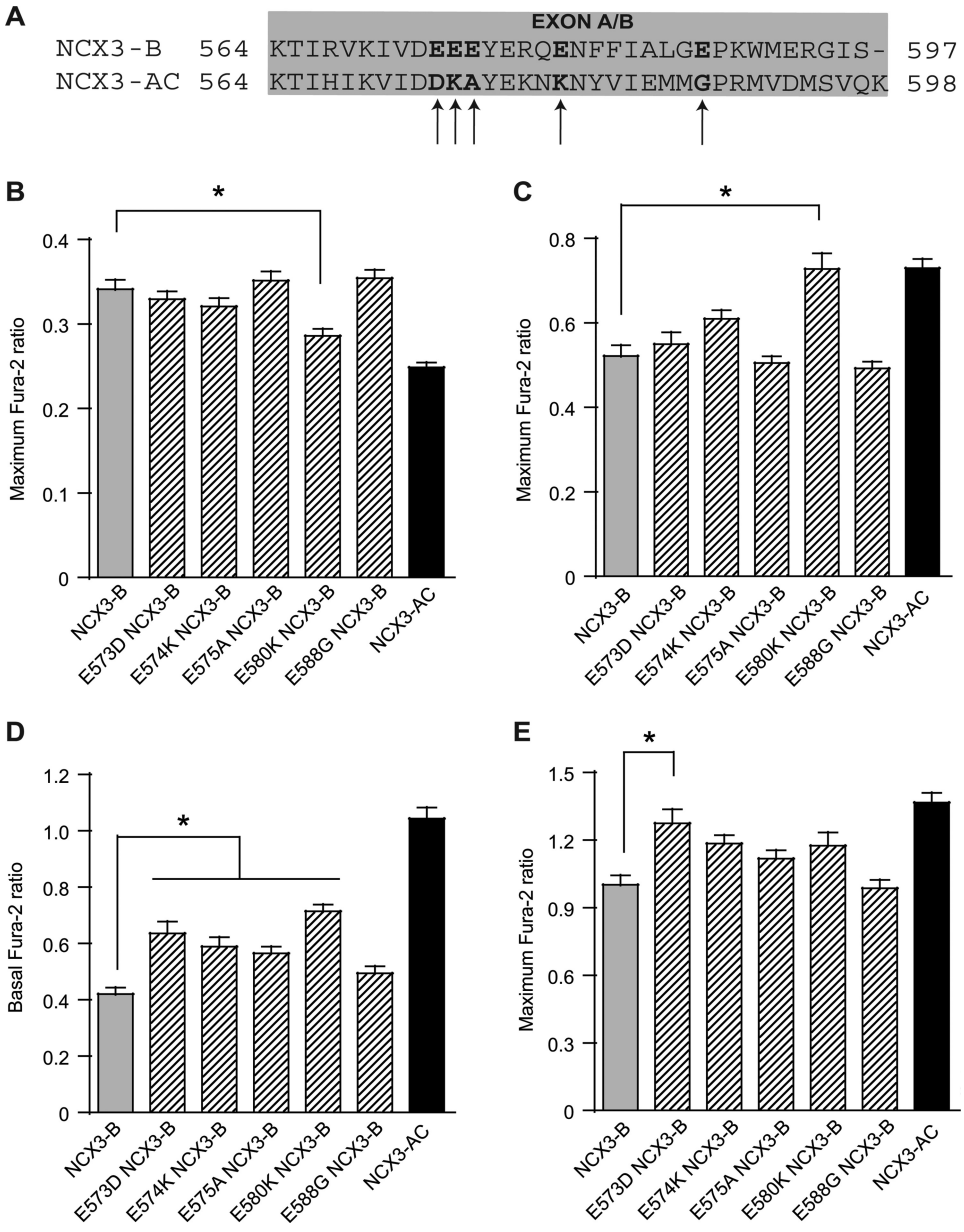


FIGURE 6. **Glutamate residues are key regulators of $Ca^{2+}$ and $Na^{+}$ sensitivity in NCX3-AC.** *A*, alignment of the amino acid sequences of the mutually exclusive exon A/B of NCX3-B to NCX3-AC. Missing residues are indicated by *dashes*. Specific NCX3-B single mutants were generated from corresponding amino acid of NCX3-AC (indicated by an *arrow*). *, $p < 0.05$ (*B–E*). *B*, mean values of the maximum Fura-2 ratio recorded during forward mode followed by the addition of ionomycin (1 $\mu$M) in $Ca^{2+}$-free conditions in cells expressing NCX3-AC, NCX3-B, or mutants of NCX3-B. NCX3-B, $n = 108$; NCX3-AC, $n = 116$; E573D NCX3-B, $n = 93$; E574K NCX3-B, $n = 110$; E575A NCX3-B, $n = 82$; E580K NCX3-B, $n = 90$; E588G NCX3-B, $n = 110$. *C*, mean values of the maximum Fura-2 ratio in reverse mode triggered by the switch to $Na^{+}$-free medium containing 1 $\mu$M thapsigargin. Values were recorded in HEK293T cells expressing NCX3 variants and mutants of NCX3-B. NCX3-B, $n = 102$; NCX3-AC, $n = 120$; E573D NCX3-B, $n = 77$; E574K NCX3-B, $n = 110$; E575A NCX3-B, $n = 121$; E580K NCX3-B, $n = 86$; E588G NCX3-B, $n = 102$. *D* and *E*, Fura-2 ratio recorded during reverse mode triggered by 1-h treatment with ouabain (1 $\mu$M) in NCX3-AC, NCX3-B, and NCX3-B mutants expressing HEK293T cells. NCX3-B, $n = 99$; NCX3-AC, $n = 88$; E573D NCX3-B, $n = 86$; E574K NCX3-B, $n = 76$; E575A NCX3-B, $n = 122$; E580K NCX3-B, $n = 123$; E588G NCX3-B, $n = 99$; *D*, mean values of Fura-2 ratio at the baseline and average of the first 60 s of the experiment in 147 mM $Na^{+}$ medium. *E*, mean values of the maximum Fura-2 ratio after the switch to $Na^{+}$-free medium during the same experiment as described in *D*.

in excitable cells (47–49). Therefore, NCX3 could in principle be involved in this process in slow-twitch muscle. Nevertheless, our study was only performed in HEK 293 cells, albeit a well used cell model to study mechanistic properties and ionic regulation of NCX isoforms (35, 50, 51). Therefore, confirmation of the latter hypothesis needs further investigations using muscular excitable tissue, in particular in soleus.

In conclusion, two variants of NCX3, which depict a tissue-specific distribution among excitable tissues, have distinct properties with regard to capacity of exchange and sensitivity to $[Ca^{2+}]_i$ and $[Na^{+}]_i$, with NCX3-AC functioning with a greater capacity in all situations. Our data indicated that NCX3-AC is the main variant expressed in skeletal muscle with a high expression in soleus, a muscle in which NCX have been shown to be implicated in the resistance to fatigue (44). Additionally, our results are, to the best of our knowledge, the first functional recordings of NCX3-AC and provides evidence of a high capacity to achieve $Ca^{2+}$ influx that can be triggered by a simple

increase in $[Na^+]_i$. This exchanger might, therefore, play a role in the resistance to muscle fatigability observed in the slow-twitch muscle. Altogether, this study provides insights into the ionic regulation of NCX3 through its alternative splicing in a tissue-specific manner. In fact, the two variants may contribute to $Ca^{2+}$ handling beyond their role in $Ca^{2+}$ extrusion.

## REFERENCES


1. Crespo, L. M., Grantham, C. J., and Cannell, M. B. (1990) Kinetics, stoichiometry and role of the Na-Ca exchange mechanism in isolated cardiac myocytes. *Nature* **345,** 618–621
2. Kimura, J., Noma, A., and Irisawa, H. (1986) Na-Ca exchange current in mammalian heart cells. *Nature* **319,** 596–597
3. Hinata, M., Yamamura, H., Li, L., Watanabe, Y., Watano, T., Imaizumi, Y., and Kimura, J. (2002) Stoichiometry of $Na^+$-$Ca^{2+}$ exchange is 3:1 in guinea-pig ventricular myocytes. *J. Physiol.* **545,** 453–461
4. Liao, J., Li, H., Zeng, W., Sauer, D. B., Belmares, R., and Jiang, Y. (2012) Structural insight into the ion-exchange mechanism of the sodium/calcium exchanger. *Science* **335,** 686–690
5. Szerencsei, R. T., Kinjo, T. G., and Schnetkamp, P. P. (2013) The topology of the C-terminal sections of the NCX1 $Na^+/Ca^{2+}$ exchanger and the NCKX2 $Na^+/Ca^{2+}$-$K^+$ exchanger. *Channels* **7,** 109–114
6. John, S. A., Liao, J., Jiang, Y., and Ottolia, M. (2013) The cardiac $Na^+$-$Ca^{2+}$ exchanger has two cytoplasmic ion permeation pathways. *Proc. Natl. Acad. Sci. U.S.A.* **110,** 7500–7505
7. Hilgemann, D. W. (1990) Regulation and deregulation of cardiac $Na^+$-$Ca^{2+}$ exchange in giant excised sarcolemmal membrane patches. *Nature* **344,** 242–245
8. Matsuoka, S., Nicoll, D. A., Hryshko, L. V., Levitsky, D. O., Weiss, J. N., and Philipson, K. D. (1995) Regulation of the cardiac $Na^+$-$Ca^{2+}$ exchanger by $Ca^{2+}$. Mutational analysis of the $Ca^{2+}$-binding domain. *J. Gen. Physiol.* **105,** 403–420
9. Hilgemann, D. W., Matsuoka, S., Nagel, G. A., and Collins, A. (1992) Steady-state and dynamic properties of cardiac sodium-calcium exchange. Sodium-dependent inactivation. *J. Gen. Physiol.* **100,** 905–932
10. Cai, X., and Lytton, J. (2004) The cation/$Ca^{2+}$ exchanger superfamily: phylogenetic analysis and structural implications. *Mol. Biol. Evol.* **21,** 1692–1703
11. Kofuji, P., Hadley, R. W., Kieval, R. S., Lederer, W. J., and Schulze, D. H. (1992) Expression of the Na-Ca exchanger in diverse tissues: a study using the cloned human cardiac Na-Ca exchanger. *Am. J. Physiol.* **263,** C1241–1249
12. Quednau, B. D., Nicoll, D. A., and Philipson, K. D. (1997) Tissue specificity and alternative splicing of the $Na^+/Ca^{2+}$ exchanger isoforms NCX1, NCX2, and NCX3 in rat. *Am. J. Physiol.* **272,** C1250–1261
13. Nicoll, D. A., Quednau, B. D., Qui, Z., Xia, Y. R., Lusis, A. J., and Philipson, K. D. (1996) Cloning of a third mammalian $Na^+$-$Ca^{2+}$ exchanger, NCX3. *J. Biol. Chem.* **271,** 24914–24921
14. Lindgren, R. M., Zhao, J., Heller, S., Berglind, H., and Nistér, M. (2005) Molecular cloning and characterization of two novel truncated isoforms of human $Na^+/Ca^{2+}$ exchanger 3, expressed in fetal brain. *Gene* **348,** 143–155
15. Secondo, A., Staiano, R. I., Scorziello, A., Sirabella, R., Boscia, F., Adornetto, A., Valsecchi, V., Molinaro, P., Canzoniero, L. M., Di Renzo, G., and Annunziato, L. (2007) BHK cells transfected with NCX3 are more resistant to hypoxia followed by reoxygenation than those transfected with NCX1 and NCX2: Possible relationship with mitochondrial membrane potential. *Cell Calcium* **42,** 521–535
16. Pannaccione, A., Secondo, A., Molinaro, P., D'Avanzo, C., Cantile, M., Esposito, A., Boscia, F., Scorziello, A., Sirabella, R., Sokolow, S., Herchuelz, A., Di Renzo, G., and Annunziato, L. (2012) A new concept: A$\beta$1–42 generates a hyperfunctional proteolytic NCX3 fragment that delays caspase-12 activation and neuronal death. *J. Neurosci.* **32,** 10609–10617
17. Huerta, M., Muñiz, J., Vásquez, C., Marin, J. L., and Trujillo, X. (1991) Sodium/calcium exchange in tonic skeletal muscle fibers of the frog. *Jpn. J. Physiol.* **41,** 933–944
18. Sokolow, S., Manto, M., Gailly, P., Molgó, J., Vandebrouck, C., Vanderwinden, J. M., Herchuelz, A., and Schurmans, S. (2004) Impaired neuromuscular transmission and skeletal muscle fiber necrosis in mice lacking Na/Ca exchanger 3. *J. Clin. Invest.* **113,** 265–273
19. Hoenderop, J. G., Hartog, A., Stuiver, M., Doucet, A., Willems, P. H., and Bindels, R. J. (2000) Localization of the epithelial $Ca^{2+}$ channel in rabbit kidney and intestine. *J. Am. Soc. Nephrol.* **11,** 1171–1178
20. van de Graaf, S. F., Hoenderop, J. G., Gkika, D., Lamers, D., Prenen, J., Rescher, U., Gerke, V., Staub, O., Nilius, B., and Bindels, R. J. (2003) Functional expression of the epithelial $Ca^{2+}$ channels (TRPV5 and TRPV6) requires association of the S100A10-annexin 2 complex. *EMBO J.* **22,** 1478–1487
21. Gkika, D., Topala, C. N., Hoenderop, J. G., and Bindels, R. J. (2006) The immunophilin FKBP52 inhibits the activity of the epithelial $Ca^{2+}$ channel TRPV5. *Am. J. Physiol. Renal Physiol.* **290,** F1253–1259
22. Kamsteeg, E. J., Wormhoudt, T. A., Rijss, J. P., van Os, C. H., and Deen, P. M. (1999) An impaired routing of wild-type aquaporin-2 after tetramerization with an aquaporin-2 mutant explains dominant nephrogenic diabetes insipidus. *EMBO J.* **18,** 2394–2400
23. Chang, Q., Hoefs, S., van der Kemp, A. W., Topala, C. N., Bindels, R. J., and Hoenderop, J. G. (2005) The $\beta$-glucuronidase klotho hydrolyzes and activates the TRPV5 channel. *Science* **310,** 490–493
24. Thurneysen, T., Nicoll, D. A., Philipson, K. D., and Porzig, H. (2002) Sodium/calcium exchanger subtypes NCX1, NCX2 and NCX3 show cell-specific expression in rat hippocampus cultures. *Brain Res. Mol. Brain Res.* **107,** 145–156
25. Lambers, T. T., Weidema, A. F., Nilius, B., Hoenderop, J. G., and Bindels, R. J. (2004) Regulation of the mouse epithelial $Ca^{2+}$ channel TRPV6 by the $Ca^{2+}$-sensor calmodulin. *J. Biol. Chem.* **279,** 28855–28861
26. Armstrong, R. B., and Phelps, R. O. (1984) Muscle fiber type composition of the rat hindlimb. *Am. J. Anat.* **171,** 259–272
27. Balasubramanyam, M., Rohowsky-Kochan, C., Reeves, J. P., and Gardner, J. P. (1994) $Na^+/Ca^{2+}$ exchange-mediated calcium entry in human lymphocytes. *J. Clin. Invest.* **94,** 2002–2008
28. Rose, C. R., and Ransom, B. R. (1996) Intracellular sodium homeostasis in rat hippocampal astrocytes. *J. Physiol.* **491,** 291–305
29. Besserer, G. M., Ottolia, M., Nicoll, D. A., Chaptal, V., Cascio, D., Philipson, K. D., and Abramson, J. (2007) The second $Ca^{2+}$-binding domain of the $Na^+$ $Ca^{2+}$ exchanger is essential for regulation: crystal structures and mutational analysis. *Proc. Natl. Acad. Sci. U.S.A.* **104,** 18467–18472
30. Hilge, M., Aelen, J., Perrakis, A., and Vuister, G. W. (2007) Structural basis for $Ca^{2+}$ regulation in the $Na^+/Ca^{2+}$ exchanger. *Ann. N.Y. Acad. Sci.* **1099,** 7–15
31. Hilge, M., Aelen, J., Foarce, A., Perrakis, A., and Vuister, G. W. (2009) $Ca^{2+}$ regulation in the $Na^+/Ca^{2+}$ exchanger features a dual electrostatic switch mechanism. *Proc. Natl. Acad. Sci. U.S.A.* **106,** 14333–14338
32. Hilge, M., Aelen, J., and Vuister, G. W. (2006) $Ca^{2+}$ regulation in the $Na^+/Ca^{2+}$ exchanger involves two markedly different $Ca^{2+}$ sensors. *Mol. Cell* **22,** 15–25
33. Breukels, V., Touw, W. G., and Vuister, G. W. (2012) Structural and dynamic aspects of $Ca^{2+}$ and $Mg^{2+}$ binding of the regulatory domains of the $Na^+/Ca^{2+}$ exchanger. *Biochem. Soc. Trans.* **40,** 409–414
34. Dyck, C., Omelchenko, A., Elias, C. L., Quednau, B. D., Philipson, K. D., Hnatowich, M., and Hryshko, L. V. (1999) Ionic regulatory properties of brain and kidney splice variants of the NCX1 $Na^+$-$Ca^{2+}$ exchanger. *J. Gen. Physiol.* **114,** 701–711
35. Hurtado, C., Prociuk, M., Maddaford, T. G., Dibrov, E., Mesaeli, N., Hryshko, L. V., and Pierce, G. N. (2006) Cells expressing unique $Na^+/Ca^{2+}$ exchange (NCX1) splice variants exhibit different susceptibilities to $Ca^{2+}$ overload. *Am. J. Physiol. Heart Circ. Physiol.* **290,** H2155–2162
36. Dunn, J., Elias, C. L., Le, H. D., Omelchenko, A., Hryshko, L. V., and Lytton, J. (2002) The molecular determinants of ionic regulatory differences between brain and kidney $Na^+/Ca^{2+}$ exchanger (NCX1) isoforms. *J. Biol. Chem.* **277,** 33957–33962
37. Fatt, P., and Katz, B. (1952) Spontaneous subthreshold activity at motor nerve endings. *J. Physiol.* **117,** 109–128
38. Rebolledo, A., Speroni, F., Raingo, J., Salemme, S. V., Tanzi, F., Munin, V., Añón, M. C., and Milesi, V. (2006) The $Na^+/Ca^{2+}$ exchanger is active and working in the reverse mode in human umbilical artery smooth muscle

cells. *Biochem. Biophys. Res. Commun.* **339,** 840–845
39. Minami, A., Xia, Y. F., and Zucker, R. S. (2007) Increased $Ca^{2+}$ influx through $Na^{+}/Ca^{2+}$ exchanger during long-term facilitation at crayfish neuromuscular junctions. *J. Physiol.* **585,** 413–427
40. Viatchenko-Karpinski, S., Terentyev, D., Jenkins, L. A., Lutherer, L. O., and Györke, S. (2005) Synergistic interactions between $Ca^{2+}$ entries through L-type $Ca^{2+}$ channels and $Na^{+}$-$Ca^{2+}$ exchanger in normal and failing rat heart. *J. Physiol.* **567,** 493–504
41. Yamamura, H., Cole, W. C., Kita, S., Hotta, S., Murata, H., Suzuki, Y., Ohya, S., Iwamoto, T., and Imaizumi, Y. (2013) Overactive bladder mediated by accelerated $Ca^{2+}$ influx mode of $Na^{+}/Ca^{2+}$ exchanger in smooth muscle. *Am. J. Physiol. Cell Physiol.* **305,** C299–308
42. Kitao, T., Takuma, K., Kawasaki, T., Inoue, Y., Ikehara, A., Nashida, T., Ago, Y., and Matsuda, T. (2010) The $Na^{+}/Ca^{2+}$ exchanger-mediated $Ca^{2+}$ influx triggers nitric oxide-induced cytotoxicity in cultured astrocytes. *Neurochem. Int.* **57,** 58–66
43. Cairns, S. P., Hing, W. A., Slack, J. R., Mills, R. G., and Loiselle, D. S. (1998) Role of extracellular [$Ca^{2+}$] in fatigue of isolated mammalian skeletal muscle. *J. Appl. Physiol.* **84,** 1395–1406
44. Germinario, E., Esposito, A., Midrio, M., Peron, S., Palade, P. T., Betto, R., and Danieli-Betto, D. (2008) High-frequency fatigue of skeletal muscle: role of extracellular $Ca^{2+}$. *Eur. J. Appl. Physiol.* **104,** 445–453
45. Jung, S. Y., Park, Y. J., Park, Y. J., Cha, S. H., Lee, M. Z., and Suh, C. K. (2007) $Na^{+}$-$Ca^{2+}$ exchanger modulates $Ca^{2+}$ content in intracellular $Ca^{2+}$ stores in rat osteoblasts. *Exp. Mol. Med.* **39,** 458–468
46. Hirota, S., Pertens, E., and Janssen, L. J. (2007) The reverse mode of the $Na^{+}/Ca^{2+}$ exchanger provides a source of $Ca^{2+}$ for store refilling following agonist-induced $Ca^{2+}$ mobilization. *Am. J. Physiol. Lung Cell. Mol. Physiol.* **292,** L438–447
47. Huang, J., Hove-Madsen, L., and Tibbits, G. F. (2007) SR $Ca^{2+}$ refilling upon depletion and SR $Ca^{2+}$ uptake rates during development in rabbit ventricular myocytes. *Am. J. Physiol. Cell Physiol.* **293,** C1906–1915
48. Piacentino, V., 3rd, Margulies, K. B., and Houser, S. R. (2002) Ca influx via the Na/Ca exchanger maintains sarcoplasmic reticulum Ca content in failing human myocytes. *Ann. N.Y. Acad. Sci.* **976,** 476–477
49. Sirabella, R., Secondo, A., Pannaccione, A., Scorziello, A., Valsecchi, V., Adornetto, A., Bilo, L., Di Renzo, G., and Annunziato, L. (2009) Anoxia-induced NF-κB-dependent upregulation of NCX1 contributes to $Ca^{2+}$ refilling into endoplasmic reticulum in cortical neurons. *Stroke* **40,** 922–929
50. Iwamoto, T., and Shigekawa, M. (1998) Differential inhibition of $Na^{+}/Ca^{2+}$ exchanger isoforms by divalent cations and isothiourea derivative. *Am. J. Physiol.* **275,** C423–430
51. John, S. A., Ribalet, B., Weiss, J. N., Philipson, K. D., and Ottolia, M. (2011) $Ca^{2+}$-dependent structural rearrangements within $Na^{+}$-$Ca^{2+}$ exchanger dimers. *Proc. Natl. Acad. Sci. U.S.A.* **108,** 1699–1704